Acta Astronautica 68 (2011) 141–148

Contents lists available at ScienceDirect

Acta Astronautica

journal homepage: www.elsevier.com/locate/actaastro

Wavefront correction of optical beam for large space mirrors using robust control techniques ☆

Jae Jun Kim *, Daniel C. Burtz, Brij N. Agrawal

Department of Mechanical and Astronautical Engineering, Naval Postgraduate School, Monterey, CA 93943, United States

ARTICLE INFO

Article history:
Received 5 February 2010
Received in revised form
27 July 2010
Accepted 28 July 2010
Available online 25 August 2010

Keywords:
Adaptive optics
Segmented mirror telescope
Robust control

ABSTRACT

For an imaging spacecraft to provide higher resolution imaging capability, the satellite will require larger mirrors. Because of the weight and launch constraints for space-based optics systems, the mirrors will have to be segmented and light-weight, resulting in increased flexibility and lower structural frequencies. Consequently, achieving surface accuracy requirements for high resolution imaging with these large aperture light-weight mirrors become a challenging task. This paper investigates the use of adaptive optics for wavefront sensing and surface control of large segmented mirrors. An H_∞ robust control technique is considered for the control of the adaptive optics system with the reduced number of inputs and outputs using singular value decomposition and Zernike polynomials. The robust controller design with the reduced model is validated with a computer simulation for a full plant in the presence of disturbances.

Published by Elsevier Ltd.

1. Introduction

For an imaging spacecraft to achieve higher resolution images, the size of the telescope aperture needs to be increased without losing accuracy in the mirror surface figure. For ground telescopes with large aperture mirrors, employing an adaptive optics system using deformable mirrors and wavefront sensors is critical to correct aberrations in the image caused by atmospheric turbulence. For space telescopes, the major source of image aberration is likely caused from the telescope structure. Because of the weight and launch constraints for space-based optics systems, the space mirrors will have to be segmented and light-weight, resulting in increased flexibility and lower structural frequencies. This structural vibration and deformation will cause aberrations in the image and degrade the imaging capabilities. Consequently, future space telescopes will require adaptive optics systems that are capable of segment alignment, optical jitter control, and surface figure control.

Many ground adaptive optics systems use simple control laws such as integral controllers based on the assumption of a static linear relationship between deformable mirror actuator inputs and wavefront sensor outputs. A control design for adaptive optics systems with large flexible mirrors is a challenging problem because of high order highly coupled system dynamics and the large number of inputs and outputs. When the dynamics of the mirror structure are ignored in the controller design, the control-structure interaction could lead to an instability of a system. Therefore, adaptive optics control design without considering mirror dynamics may not be valid for large flexible space mirrors.

Control of large flexible space structures has been a constant subject of research. Safonov et al. [1] synthesized the H_∞ robust controller for a large space telescope structure model with 58 vibration modes. The paper addresses various issues in robust controller design such as pre-conditioning of the plant, model reduction, and

☆ This paper was presented during the 60th IAC in Daejeon.

* Corresponding author.
E-mail address: jki1@nps.edu (J.J. Kim).

0094-5765/$ - see front matter Published by Elsevier Ltd.
doi:10.1016/j.actaastro.2010.07.017

robustness. H_∞ robust control design is also studied for the Advanced Structure/Control Integrated Experiment (ASCIE) consisting of hexagonal mirror segments for the primary optic and a lightweight truss support structure [2,3]. The ASCIE has 18 actuator inputs, 24 sensor outputs, and only considers the piston, tip, and tilt correction of each segments. Centralized, decentralized, and overlapping control architectures to handle the complexity of ASCIE are presented in [2]. Rigorous analysis on modeling and robust control techniques for ASCIE is presented in [3].

Robust control design is also considered for adaptive optics systems with deformable mirror surfaces. Frazier et al. applied the robust control technique for an adaptive optics testbed with a 37 channel deformable mirror [4–7]. Other works have begun to apply advanced control techniques to large ground based telescopes that have more structural flexibility than previous generation telescopes, similar to what space-based telescopes will experience [8–10].

In this paper, we investigate the adaptive optics system of a large segmented mirror space telescope and its control design using the H_∞ robust control technique. Model reduction is also performed for the robust control design including the reduction of the number of inputs and outputs using the singular value decomposition and Zernike polynomials. Computer simulation results are also provided for the proposed control design.

2. Adaptive optics for segmented space telescope

The term adaptive optics refers to any optical system in which some optical component; be it a mirror, lens, or some other device, undergoes adaptation or modification to improve the resulting wavefront. The optical wavefront is a surface formed by a collection of points of a propagating beam with the same phase. The wavefront is measured by a wavefront sensing device such as a Shack Hartmann wavefront sensor. Ideally, the wavefront from a distant point source travelling through a vacuum without any interference would be planar, or flat. In reality, various aberrations cause the wavefront to be non-planar. As the light propagates though a dynamic atmosphere, or any other medium, it becomes aberrated to an observer on the other side of that medium. Other aberrations arise from imperfections in optical components, such as uneven coatings, imperfect shapes, or impurities in glass, among others. A moving or vibrating platform can also lead to wavefront aberrations, which is of particular concern for large space telescopes.

Adaptive optics systems typically consist of a wavefront sensor, an adaptive optical component, and a control computer. Fig. 1 shows the simplified schematic of the adaptive optics system for segmented space telescope where the deformable primary mirror is used to correct aberrations. The wavefront sensor requires a reference beam such as a beacon, a laser source, a bright star next to the object, or an object itself which contains aberration information.

The most common wavefront sensor for adaptive optics systems is the Shack–Hartmann wavefront sensor. It consists of a camera and a lenslet array at the front entrance pupil of the camera. Each of these lenslets is identical and will focus the incoming light on the imaging chip behind it. For a planar incoming wavefront, the location of the focused spots on the CCD will be evenly spaced in the same geometric pattern as the lenslet array. When the incoming wavefront is not planar, the focused spots will have displacements on the CCD as shown in Fig. 2, which is proportional to the local slope of the incoming wavefront.

Fig. 3 shows the configuration of the actuators and sensors of the segmented telescope model considered in this paper. The primary optic of the telescope consists of six hexagonal segments. Each segment has 156 facesheet actuators physically integrated into the mirror segment structure for a total of 936 actuators. There are 61 lenslets

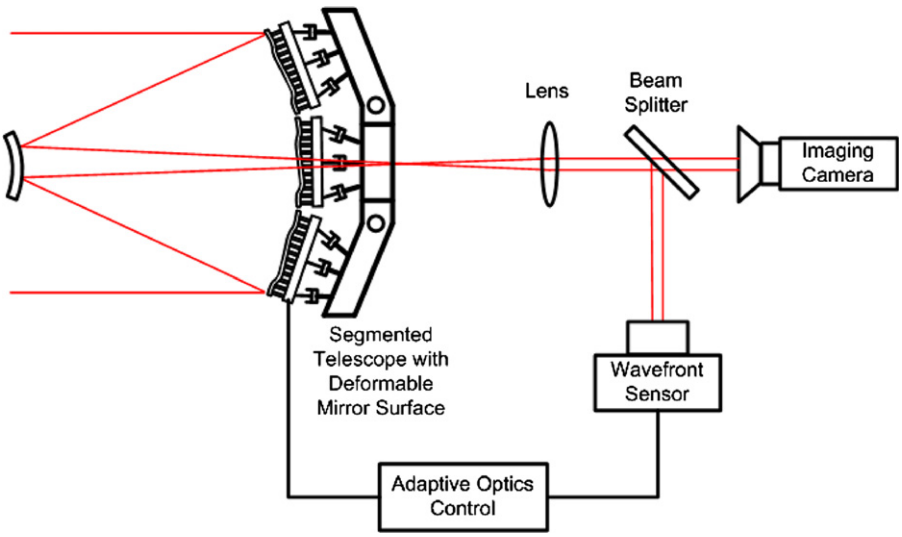

Fig. 1. Adaptive optics system of a segmented telescope.

in each of the six Shack Hartmann sensors, for a total of 366 lenslets. Each Shack Hartmann sensor is optically mapped to each segment as shown in Fig. 3. The Shack Hartmann sensor outputs are given as groups of x-slopes and y-slopes for each segment.

For an adaptive optics control design, the system plant can be simply modeled as a static linear relation between input and output,

$$\mathbf{y} = \mathbf{\Phi u} \tag{1}$$

where y is the Shack Hartmann sensor output, u is the actuator control input, and $\mathbf{\Phi}$ is the influence matrix, which is also called the poke matrix since $\mathbf{\Phi}$ can be determined experimentally by poking each actuator and observing the sensor output. For this simple plant, the integral controller in discrete time becomes

$$\mathbf{u}(k) = \mathbf{u}(k-1) - \mu \mathbf{\Phi}^{\dagger} \mathbf{y}(k) \tag{2}$$

where $\mathbf{\Phi}^{\dagger}$ represents pseudo-inverse of the poke matrix, μ is the adaptation gain, and k is the time index. When the number of sensor measurements is larger than the number of actuator inputs, the pseudo-inverse provides the least squares solution of the control input required. When the number of actuator inputs is larger than the number of sensor measurement, the pseudo-inverse provides the minimum-norm solution. This simple integral controller ignores the structural dynamics of a system and therefore it has a limited performance. A robust controller for adaptive optics system is attractive when the dynamics of the system are accounted for since it can handle MIMO systems in the presence of external disturbances and unmodeled dynamics.

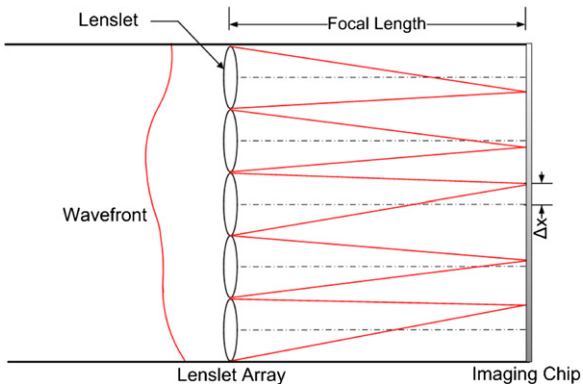

Fig. 2. Shack Hartmann wavefront sensor.

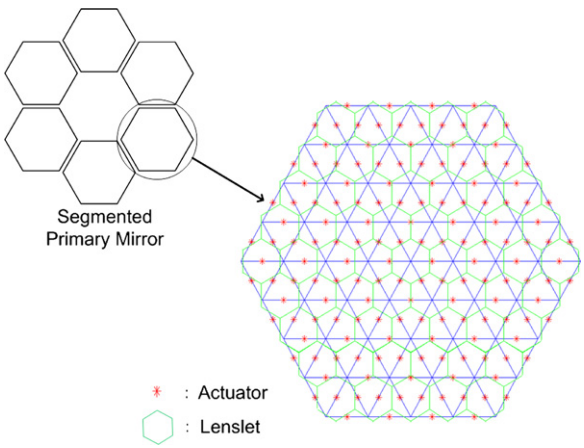

Fig. 3. Locations of actuators and Shack–Hartmann lenslets of a mirror segment.

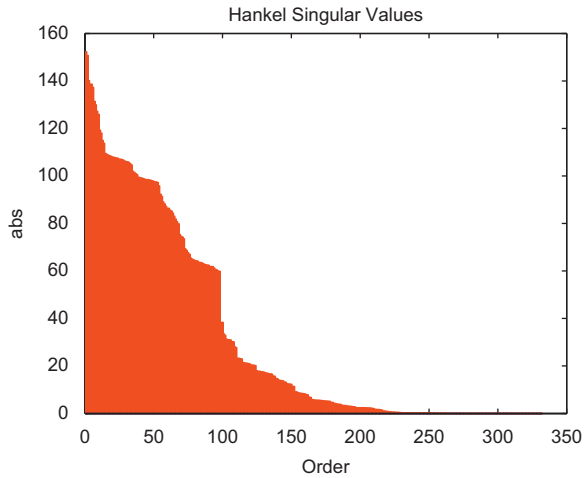

Fig. 4. Hankel singular values.

3. H_∞ robust control design

3.1. Modeling of segmented mirror telescope

The segmented mirror telescope model was generated using a finite element program by Lockheed Martin. Only the first 166 vibration modes with frequencies ranging from 29.1 to 767.6 Hz were retained in the model represented in modal coordinates. The damping ratio is 0.3 for all the frequency modes. In addition to the 936 facesheet actuators and 732 Shack–Hartmann sensor outputs, the simulation model also includes additional sensors and actuators for optical jitter control and segment alignments. It is assumed that the controller for optical jitter and segment alignment can be designed separately from the adaptive optics controller with facesheet actuators and Shack Hartmann sensors. This is a reasonable assumption since the targeting control bandwidth is significantly different for each control design. The plant of the adaptive optics system can be represented in state space form.

$$\dot{\mathbf{x}} = \mathbf{Ax} + \mathbf{Bu}$$

$$\mathbf{y} = \mathbf{Cx} + \mathbf{Du} \tag{3}$$

where $A \in \mathcal{R}^{332\times332}$, $B \in \mathcal{R}^{332\times936}$, $C \in \mathcal{R}^{732\times332}$, $D \in \mathcal{R}^{732\times936}$, $\mathbf{x}$ is the state variable, $\mathbf{y}$ is the measured output, and $\mathbf{u}$ is the control input. In the frequency domain, the output of the system is

$$\mathbf{Y}(s) = [\mathbf{C}(s\mathbf{I}-\mathbf{A})^{-1}\mathbf{B} + \mathbf{D}]\,\mathbf{U}(s) \tag{4}$$

When the system approaches to steady-state ($s \to 0$), the DC gain of the output becomes

$$\mathbf{y} = [-\mathbf{C}\mathbf{A}^{-1}\mathbf{B} + \mathbf{D}]\,\mathbf{u} \tag{5}$$

The poke matrix in Eq. (1) can be written as

$$\mathbf{\Phi} = -\mathbf{C}\mathbf{A}^{-1}\mathbf{B} + \mathbf{D} \tag{6}$$

which is a steady-state approximation of the dynamic plant.

3.2. Model reduction

Robust control design for the plant in Eq. (3) is inhibitive due to the size of the plant. The system states can be reduced by observing Hankel singular values based on the observability and controllability grammians of the plant model. The Hankel singular values of the Segmented Mirror Telescope are plotted in Fig. 4.

Although there are 332 states present in the system, Fig. 4 shows that the number of states can be reduced to about 240 without losing significant information in the system, since the Hankel singular values have close to zero influence on the system above 240. This reduced state model is used for controller synthesis.

3.3. Input/output reduction

Input/output reduction reduces the number of inputs and outputs to the system, but does not change the internal dynamics of the system. There are two different bases for model reduction used in this paper: singular value decomposition and Zernike polynomials. Using the singular value decomposition, the poke matrix can be written as

$$\mathbf{\Phi} = \mathbf{U}\mathbf{\Sigma}\mathbf{V}^{\mathrm{T}} \tag{7}$$

where $\mathbf{U}$ and $\mathbf{V}$ are unitary matrices and $\mathbf{\Sigma}$ is a diagonal matrix with singular values on the diagonal. The columns $\mathbf{u}_1,\ldots,\mathbf{u}_m$ of $\mathbf{U}$ and $\mathbf{v}_1,\ldots,\mathbf{v}_m$ of $\mathbf{V}$ can provide orthonormal basis for the linear transformation $\mathbf{y} = \mathbf{\Phi}\mathbf{u}$. This transformation maps the ith basis vector $\mathbf{u}_i$ to the ith basis vector $\mathbf{v}_i$ with the magnitude of the ith singular value σ_i. For the segmented mirror telescope model, first 21 terms are retained in the reduced model. The input/output reduced model is written as

$$\dot{\mathbf{x}} = \mathbf{A}\mathbf{x} + \mathbf{B}\mathbf{M}\bar{\mathbf{u}}$$

$$\bar{\mathbf{y}} = \mathbf{P}\mathbf{C}\mathbf{x} + \mathbf{P}\mathbf{D}\mathbf{M}\bar{\mathbf{u}} \tag{8}$$

where

$$\mathbf{u} = \mathbf{M}\bar{\mathbf{u}} \quad \bar{\mathbf{y}} = \mathbf{P}\mathbf{y}$$

$$\mathbf{M} = [\mathbf{v}_1 \cdots \mathbf{v}_{21}], \quad \mathbf{P} = [\mathbf{u}_1 \cdots \mathbf{u}_{21}]^{\mathrm{T}} \tag{9}$$

Fig. 5 shows the open loop bode plot of the reduced plant model represented in Eq. (8).

Another method for input/output reduction is using Zernike polynomials. Zernike polynomials are sequence of orthogonal polynomials defined over a unit circle to represent wavefront phase.

$$\varphi(r,\theta) = A_{00} + \frac{1}{\sqrt{2}}\sum_{n=2}^{\infty} A_{n0}\Re_n^0\left(\frac{r}{R}\right) + \sum_{n=1}^{\infty}\sum_{m=1}^{n}(A_{nm}\cos(m\theta) + B_{nm}\sin(m\theta))\Re_n^m\left(\frac{r}{R}\right) \tag{10}$$

where $\varphi(r,\theta)$ is a wavefront phase represented in polar coordinates system, R is the maximum radius of the beam for normalization, A and B are coefficients, and

$$\Re_n^m\left(\frac{r}{R}\right) = \sum_{s=0}^{(n-m)/2}(-1)^s\frac{(n-s)!}{s!\left(\frac{n+m}{2}-s\right)!\left(\frac{n-m}{2}-s\right)!}\left(\frac{r}{R}\right)^{n-2s} \tag{11}$$

There is an inverse relationship between the coefficients of the Zernike polynomials and the amount of influence that they have on the wavefront. The lower the order of polynomial coefficients, the more influence the particular coefficient has over the wavefront. Zernike polynomials in the polar coordinates can be transformed into Cartesian coordinates using $r = \sqrt{x^2+y^2}$ and $\theta = \tan^{-1}(x/y)$. The 21 most influential Zernike polynomial terms were retained in the reduced model. The Shack Hartmann wavefront sensor measures local slopes of a wavefront and the piston term (n=m=0) which the Shack Hartmann sensor cannot measure is not included in the 21 terms. The wavefront slopes in Cartesian coordinates can be written as

$$\frac{\partial\varphi(x,y)}{\partial x} = \left[\frac{\partial z_1(x,y)}{\partial x}\cdots\frac{\partial z_{21}(x,y)}{\partial x}\right]\mathbf{a}$$

$$\frac{\partial\varphi(x,y)}{\partial y} = \left[\frac{\partial z_1(x,y)}{\partial y}\cdots\frac{\partial z_{21}(x,y)}{\partial y}\right]\mathbf{a} \tag{12}$$

where $z_i(x,y)$ is the ith Zernike polynomial term and $\mathbf{a}$ is a vector of 21 Zernike polynomial coefficients. The output of the system can be written as

$$\mathbf{y} = \mathbf{Z}'\mathbf{a} \tag{13}$$

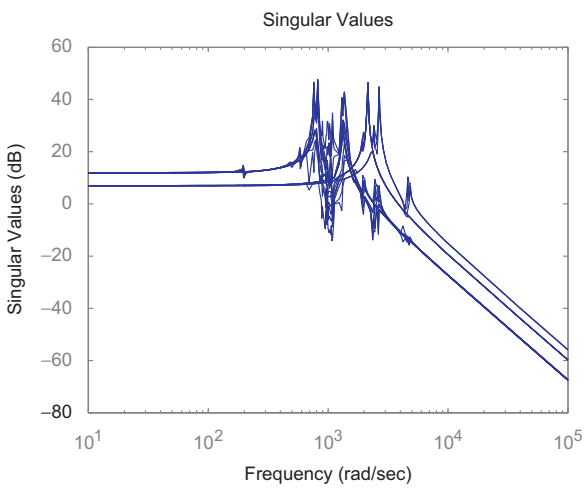

Fig. 5. Open-loop Bode plot of reduced model using SVD.

where

$$\mathbf{Z}' = \begin{bmatrix} \left.\frac{\partial z_1}{\partial x}\right|_{l_1} & \cdots & \left.\frac{\partial z_{21}}{\partial x}\right|_{l_1} \\ \vdots & \ddots & \vdots \\ \left.\frac{\partial z_1}{\partial x}\right|_{l_{366}} & \cdots & \left.\frac{\partial z_{21}}{\partial x}\right|_{l_{366}} \\ \left.\frac{\partial z_1}{\partial y}\right|_{l_1} & \cdots & \left.\frac{\partial z_{21}}{\partial y}\right|_{l_1} \\ \vdots & \ddots & \vdots \\ \left.\frac{\partial z_1}{\partial y}\right|_{l_{366}} & \cdots & \left.\frac{\partial z_{21}}{\partial y}\right|_{l_{366}} \end{bmatrix} \tag{14}$$

which is determined by evaluating x and y gradients of Zernike polynomials for all 366 lenslets. Using Eq. (13), the equation of motion can be reduced to

$$\dot{\mathbf{x}} = \mathbf{A}\mathbf{x} + \mathbf{B}\mathbf{u}$$

$$\mathbf{a} = \mathbf{Z}'^{\dagger}\mathbf{C}\mathbf{x} + \mathbf{Z}'^{\dagger}\mathbf{D}\mathbf{u} \tag{15}$$

when $s \to 0$, the transfer function of the system becomes

$$\mathbf{\Phi}' = -\mathbf{Z}'^{\dagger}\mathbf{C}\mathbf{A}\mathbf{B} + \mathbf{Z}'^{\dagger}\mathbf{D} \tag{16}$$

The system equation of motion is further reduced using the singular value decomposition, $\mathbf{\Phi}' = \mathbf{U}'\mathbf{\Sigma}'\mathbf{V}'^{\mathrm{T}}$.

$$\dot{\mathbf{x}} = \mathbf{A}\mathbf{x} + \mathbf{B}\mathbf{M}'\mathbf{u}'$$

$$\mathbf{y}' = \mathbf{Z}'^{\dagger}\mathbf{C}\mathbf{x} + \mathbf{Z}'^{\dagger}\mathbf{D}\mathbf{M}'\mathbf{u}' \tag{17}$$

where

$$\mathbf{u} = \mathbf{M}'\mathbf{u}', \quad \mathbf{M}' = [\mathbf{v}'_1 \cdots \mathbf{v}'_{21}] \tag{18}$$

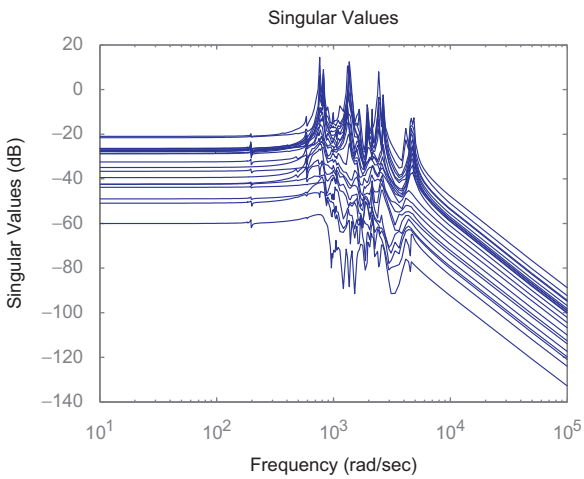

Fig. 6. Open-loop Bode plot of reduced model using Zernike polynomials and SVD.

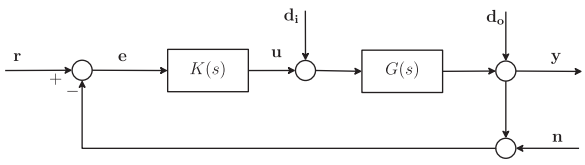

Fig. 7. Block diagram of control system.

Fig. 6 shows the open loop Bode plot of the reduced plant model represented in Eq. (17).

3.4. Control design

Fig. 7 is the block diagram of the control system where $G(s)$ represents the transfer function of the full plant, $K(s)$ represents the transfer function of the controller, $\mathbf{n}$

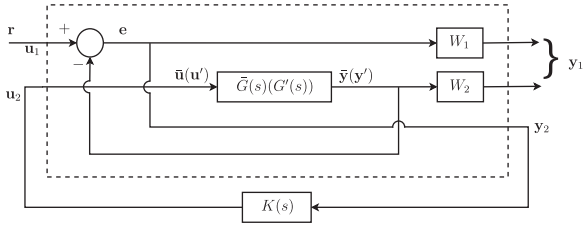

Fig. 8. Augmented plant and H_∞ controller for robust control design.

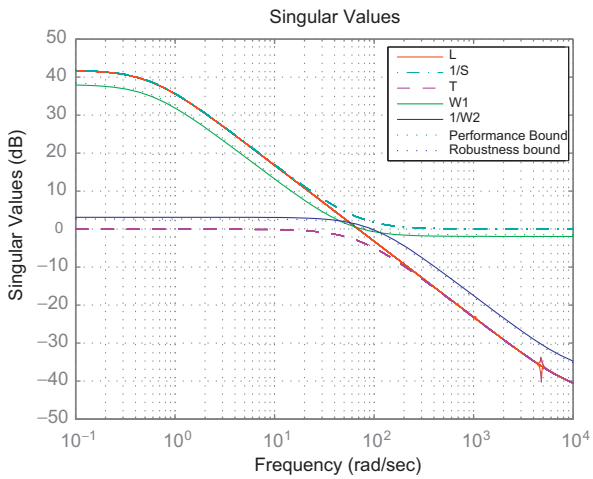

Fig. 9. Loop shape of H_∞ control system using SVD reduced model.

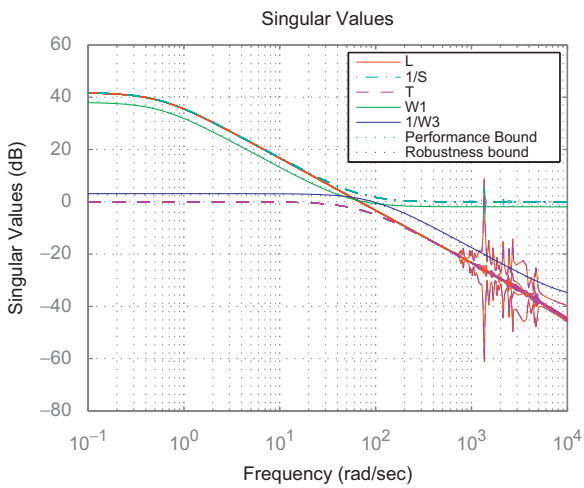

Fig. 10. Loop shape of H_∞ control system using Zernike/SVD reduced model.

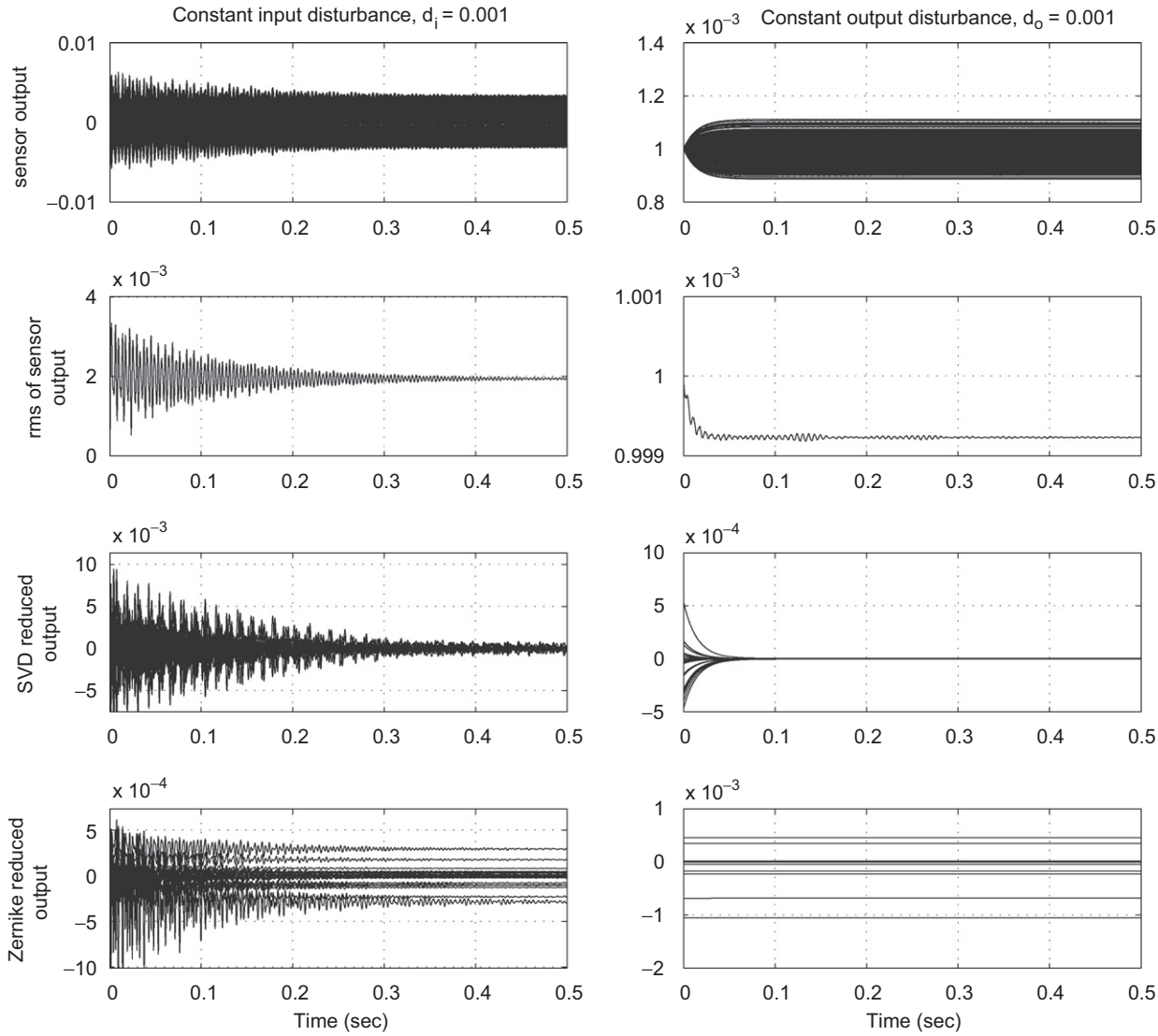

Fig. 11. Simulation results with H_∞ controller using $\overline{G}(s)$.

represents the sensor noise, $\mathbf{d_i}$ represents input disturbance, and $\mathbf{d_o}$ represents output disturbance. The control design is based on the mixed-sensitivity H_∞ approach of robust control.

Let us define the sensitivity transfer function as $S(s) = (I+G(s)K(s))^{-1}$, and the complimentary sensitivity transfer function as $T(s)=I-S(s)$. The effects on the output by disturbance can be reduced by minimizing the sensitivity function $S(s)$, but that of the effect from sensor noise n can be reduced by minimizing the complementary sensitivity function $T(s)$. Since $S(s)+T(s)=I$, both minimizations cannot be done simultaneously. In order to do this, we can design a desired loop shape by choosing proper weighting function $W_1(s)$ and $W_2(s)$ for sensitivity and complementary sensitivity functions. For the control design, the plant is augmented with the weights $W_1(s)$ and $W_2(s)$ as shown in Fig. 8. The transfer function from $\mathbf{u}_1$ to $\mathbf{y}_1$ in Fig. 8 becomes

$$T = \begin{bmatrix} W_1(s)S(s) \\ W_2(s)T(s) \end{bmatrix} \tag{19}$$

The controller transfer function is determined by the following minimization problem

$$\min_{K(s)} \left\| \begin{matrix} \gamma W_1(s)S(s) \\ W_2(s)T(s) \end{matrix} \right\|_\infty \tag{20}$$

where γ is a design parameter. For the controller design, reduced plant models with the singular value decomposition defined as $\overline{G}(s)$ and Zernike polynomials defined as $G'(s)$ are used. Robust control toolbox in Matlab is used for synthesis of the controller. Fig. 9 shows the resulting control design with weights $W_1(s)$ and $1/W_2(s)$ using the reduced model with the singular value

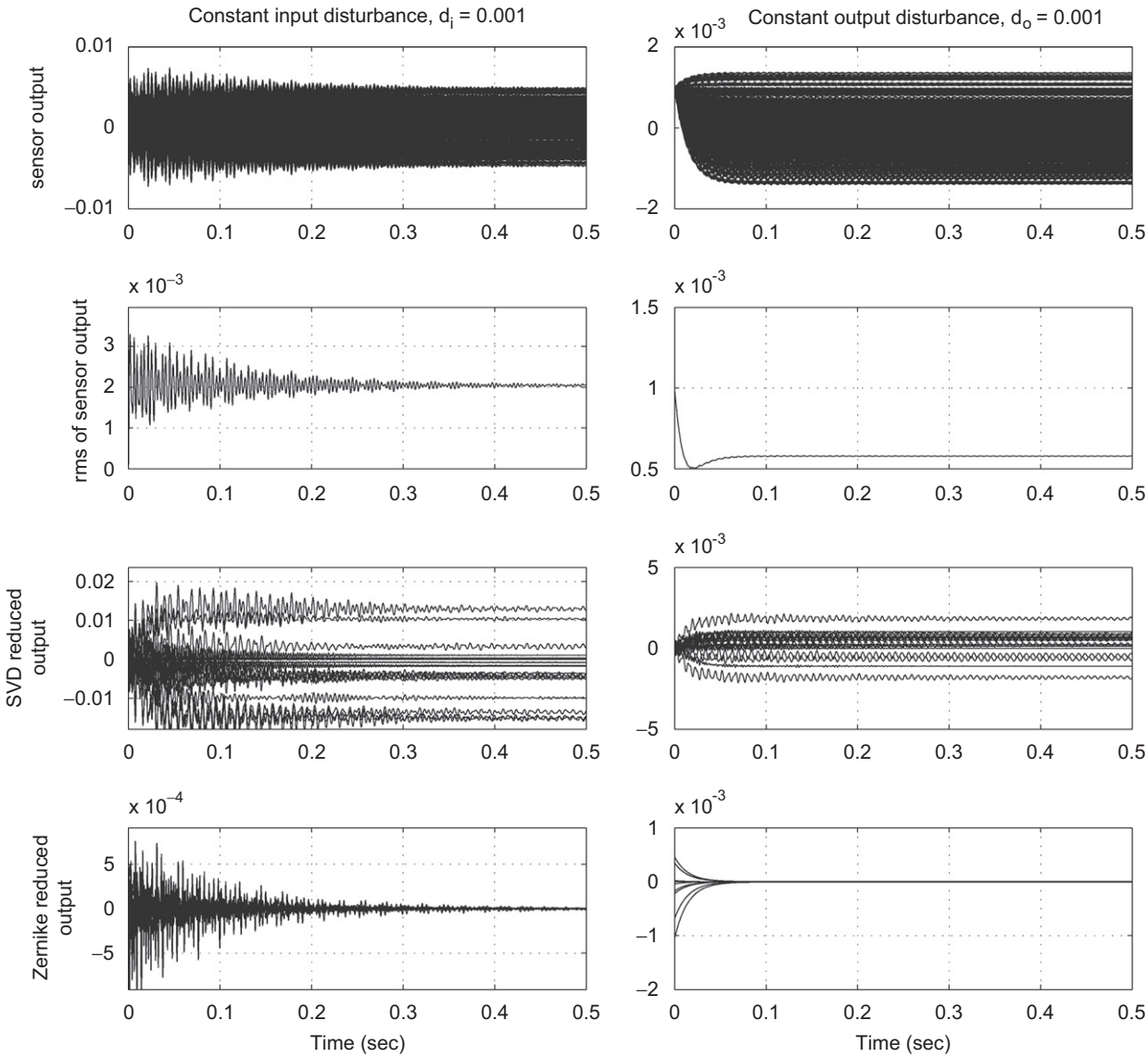

Fig. 12. Simulation results with H_∞ controller using $G'(s)$.

decomposition, $\overline{G}(s)$, where $L(s)$ represent the resulting open-loop shape. Fig. 10 is the resulting control design using the reduced model with the Zernike polynomials, $G'(s)$.

3.5. Simulation results

Computer simulation is performed on the full plant model using two H_∞ controllers with $\overline{G}(s)$ and $G'(s)$. Fig. 11 shows the output results using the controller designed for $\overline{G}(s)$ when the two disturbance sources are considered. The figures on the left column are simulation results with a constant input disturbance of d=0.001 for all control inputs. The figures on the right column shows simulation results with a constant output disturbance directly of d=0.001 directly added to all the Shack Hartmann sensor measurements. As expected, the reduced output, $\overline{\mathbf{y}}$, is converged towards zero for both cases. With the controller designed with the reduced model, the actual Shack Hartman sensor output converges to non-zero values. The root-mean-square value of the full sensor output is also shown in Fig. 11.

The more results are obtained when the full Shack–Hartmann sensor output is converted to wavefront using Zernike polynomials. The coefficients of the first 21 Zernike terms shown in Fig. 11 converges to non-zero values. Although the input/output reduction is performed with the basis that has most influence based on singular value decomposition of the poke matrix, the resulting controller based on $\overline{G}(s)$ did not impact the Zernike modes especially when the constant output disturbance is applied.

Fig. 12 shows the simulation results using the controller designed for $G'(s)$. It can be seen that the

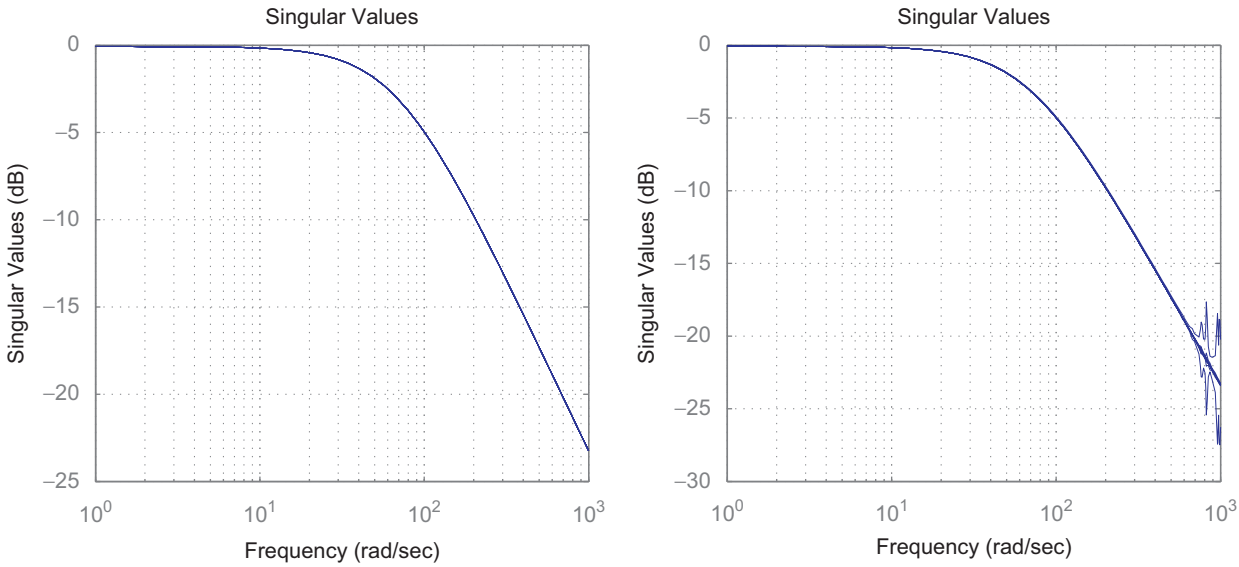

Fig. 13. Singular value Bode plots for closed loop system with $\overline{G}(s)$ (left) and $G'(s)$ (right).

reduced output, $\mathbf{y}'$, which is coefficients of first 21 Zernike polynomials, converges towards zero as expected. Since the lower order Zernike terms has more influence on the wavefront of a beam, it is anticipated that the controller designed with $G'(s)$ results in a better imaging resolution than the controller designed with $\overline{G}(s)$.

With the classical integral controller shown in Eq. (2), the targeted control bandwidth of 10 Hz cannot be easily met without adding additional structural filters or low-pass filters. Increasing the classical controller gain without structural filters would eventually make the system unstable. The classical controller design also requires input/output reduction due to the dimension of the problem. The singular value bode diagrams of the H_∞ closed loop systems with the reduced plant models, $\overline{G}(s)$ and $G'(s)$, are shown in Fig. 13, and the required 10 Hz control bandwidth can be easily attained with the H_∞ robust control design for the reduced outputs.

4. Conclusion

In this paper, an H_∞ robust control design of the space telescope adaptive optics system is presented. Due to the overall dimension of the plant, model reduction including input/output reduction is performed using the singular value decomposition and Zernike polynomials. The simulation results show that the H_∞ controllers using both reduction methods yields good performance for reduced outputs. Therefore, it is critical to choose a good basis for model reduction such that the reduced output faithfully represents the actual system output which will influence the overall system performance. Zernike polynomials form a good basis for model reduction since they are of the same form as the types of wavefront aberrations often observed in optical systems.

References

[1] M.G. Safonov, R.Y. Chiang, H. Flashner, H_∞ robust control synthesis for a large space structure, Journal of Guidance 14 (3) (1991) 513–520.
[2] K. Li, E.B. Kosmatopoulos, P.A. Ioannou, H. Ryaciotaki-Boussalis, Large segmented telescopes, centralized, decentralized, and overlapping control designs, IEEE Control Systems Magazine (2002) 59–72.
[3] A. Carrier, Modeling and shape control of a segmented-mirror telescope, Ph.D. Dissertation, Stanford University, Palo Alto, CA, 1990; M. Allen, Wavefront control for space telescope applications using adaptive optics, M.S. Thesis, Naval Postgraduate School, Monterey, CA, 2007.
[4] B.W. Frazier, R.K. Tyson, Robust control of an adaptive optics system, in: IEEE Proceedings of the 34th Southeastern Symposium on System Theory, , November 2002, pp. 293–296.
[5] B.W. Frazier, R.K. Tyson, J. Ackman, M. Smith, Closed loop results of a compact high-speed adaptive optics system with H_∞ control, Proceedings of SPIE 5169 (2003) 37–42.
[6] B.W. Frazier, J. Roche, R.K. Tyson, Y.P. Kakad, B.G. Sherlock, Robust control of an adaptive optical system, Proceedings of the Institution of Mechanical Engineers 218 (2004) 353–358.
[7] B.W. Frazier, R.K. Tyson, M. Smith, J. Roche, Theory and operation of a robust controller for a compact adaptive optics system, Optical Engineering 43 (12) (2004) 2912–2920.
[8] D.W. Miller, S.C.O. Grocott, Robust control of the multiple mirror telescope adaptive secondary mirror, Society of Photo-Optical Instrumentation Engineers 38 (8) (1999) 1276–1287.
[9] M. Whorton, G. Angeli, Modern control for the secondary mirror of a Giant segmented mirror telescope, in: SPIE Future Giant Telescopes Conference, SPIE 4840-23, August 2002.
[10] L. Baudouin, C. Prieur, F. Guignard, D. Arzelier, Robust control of a bimorph mirror for adaptive optics system, Optical Society of America Journal of Applied Optics 47 (20) (2008) 3637–3645.